Analyzing powers for the $^{12}C(^6\vec{Li},\alpha)^{14}N^*$ reaction at 33 MeV

A. J. Mendez,* K. W. Kemper, P. V. Green, P. L. Kerr, E. G. Myers, E. L. Reber,† and D. Robson
Department of Physics, Florida State University, Tallahassee, Florida 32306-3016
(Received 6 May 1994)

Angular distributions of the cross section and the first complete set of analyzing powers for $^{12}C(^6\vec{Li},\alpha)^{14}N$ have been measured over the range $4° \leq \theta_{lab} \leq 29°$ at a bombarding energy of 33 MeV. The $^TT_{20}$ analyzing power data are shown to distinguish between natural and unnatural parity states in ^{14}N as observed earlier in $(\vec{d},\alpha)$ reactions. General rules are presented for tensor analyzing powers for transfers to $0^\pm$ and $1^\pm$ states that are derived assuming only conservation of parity and total angular momentum. Finite-range deuteron cluster transfer DWBA calculations which allowed coherent multiple L transfers were carried out and compared with the data. The analyzing powers exhibited sensitivity to L mixing including the presence of D states in both ^6Li and ^{14}N but had limited success in describing the data.

PACS number(s): 24.70.+s, 25.10.+s, 24.10.Eq, 27.20.+n

I. INTRODUCTION

The $^{12}C(^6Li,\alpha)^{14}N$ reaction has been studied over a wide range of energies, from below [1] and near [2–7] the Coulomb barrier using unpolarized beams, to well above the barrier at 33 MeV [8,9]. In early studies, spectroscopy using the $(^6Li,\alpha)$ reaction was hampered by uncertainties in the reaction mechanism involved. The study of Ref. [10] concluded that the angular distributions at 20 MeV were dominated neither by purely direct nor by purely compound nuclear reaction mechanisms. However, more recent work using vector polarized ^6Li at 20 MeV [11] found justification for describing the data as a direct deuteron cluster transfer [12].

White *et al.* [8,9] studied the reaction at 33 MeV and showed that at this higher energy the direct process dominates. In their work, the measured excitation functions were relatively featureless, the angular distributions were forward peaked, and the results of Hauser-Feshbach calculations showed the compound nuclear contribution to be negligible, all indicating that the reaction was indeed direct. However, they were unable to reproduce the angular distribution data with exact finite-range DWBA calculations. These calculations gave reasonable fits only to the forward angle cross sections of the low-lying positive parity states. The negative parity states were poorly described over the entire angular range. These results led to the conclusion that the observed transitions are not dominated by a single value of orbital angular momentum in contrast with the $^{12}C(^3He,p)^{14}N$ reaction [13], where the angular distributions for all the transitions were shown to be dominated by a single L transfer, even those with two allowed values. This difference led White *et al.* to conclude that multistep mechanisms and/or contributions from the D-state component in the ^6Li wave function may be important for at least some of the transitions.

The present work reports the first complete set of analyzing powers (AP) for the $(^6\vec{Li},\alpha)$ reaction. In previous $(\vec{d},\alpha)$ studies, the AP have proven to be a very powerful spectroscopic tool because, in addition to being considerably more sensitive to the strengths of the L transfers than the cross section, they are also sensitive to the relative sign of the amplitudes, since they are formed with coherent summations over the L transfers [14,15]. While no obvious signatures appear in the data that allow the final J^π to be determined, it was found that $^TT_{20}$ $(= A_{yy}/\sqrt{2})$ is always positive for unnatural parity over a wide angular range. This result is the same as observed in $(\vec{d},\alpha)$ reactions. Rules have been developed based purely on conservation of angular momentum and parity that predict the signs of the tensor analyzing powers and ranges of allowed values for them.

Finite-range DWBA cluster transfer calculations have been carried out for the data. Extensive results for the four 1^+ states at E_x=0.00, 3.95, 6.20, and 9.70 MeV are presented and compared with the data. These calculations show that the analyzing powers are sensitive to the presence of the ^6Li D state and to L mixing in the transitions to ^{14}N states.

II. EXPERIMENTAL PROCEDURE

The $^6\vec{Li}^-$ beam was produced by the laser optically pumped polarized lithium ion source (OPPLIS, described in Refs. [16,17]) at the Florida State University tandem Van de Graaff superconducting linear accelerator laboratory. Targets of self-supporting natural carbon approximately 130 $\mu g/cm^2$ in thickness were bombarded by typically 100–150 nA of $^6\vec{Li}^{3+}$ at 33 MeV. Average beam

*Present address: University of North Carolina at Chapel Hill and Triangle Universities Nuclear Laboratory, Box 90308, Durham, NC 27708-0308.
†Present address: Idaho Falls Engineering Laboratory, Idaho Falls, Idaho 83415-2114.

polarizations were measured as discussed in Refs. [16,18] to be t_{10}=0.94±0.08 for the N_+ polarization state and t_{20}=−0.938±0.013 for the N_0 polarization state. Continuous monitoring by a helium gas polarimeter showed the on-target polarizations to vary by less than 5% over the course of the experiments.

In all measurements, α particles were stopped in silicon surface barrier detectors mounted symmetrically to the left and right of the incident beam direction. The scattering chamber had two detector wedges, each containing three detectors spaced 7.5° apart. The large Q value of the reaction allowed the α groups to be observed without using particle identification for all states of interest except for the 9.70 MeV state. Counter E-ΔE telescopes were not used so that sufficient energy resolution could be obtained to separate all states up to the 6.45 MeV state. The detectors were collimated to an angular acceptance of 0.6° to limit kinematic broadening of the line shapes. A typical spectrum from this reaction is shown in Fig. 1. Because of the highly oscillatory nature of the analyzing powers, the angular position of the left and right detectors had to be carefully calibrated. This was accomplished using the ^{6}Li + ^{12}C elastic scattering angular distribution at $E_{\rm Li}$=30 MeV, which was measured to high precision by Vineyard *et al.* [19]. By comparing left and right angular distributions, the two detectors of a left/right pair could be positioned to within ±0.2° of the same angle.

Three different polarization configurations were used for the measurements. In the first experiment, a simultaneous measurement of the quantities $t_{10}iT_{11}$ and $t_{20}{}^TT_{20}$ was performed. The source was cycled through the *off*, N_+, and N_0 states with the spin oriented vertically (β=90°, ϕ=0°) by a Wien Filter. The second experiment measured $t_{20}T_{20}$ using a polarization state sequence of *off*, N_0 with the spin oriented parallel to the incident beam (β=0°). The third experiment measured $t_{20}T_{21}$ also using a polarization state sequence of *off*, N_0, but with the spin in the horizontal reaction plane oriented at 45° to the incident beam direction (β=45°, ϕ=90°). In all three experiments, angular distributions were measured in 1° − 2° steps for $\theta_{\rm lab}$ = 8° − 29°. Additionally, unpolarized cross sections for the ground and 3.95 MeV states were measured at 4° and 6° since the forward angle portion of the cross section distributions exhibits the greatest sensitivity to the L transfers. The cross sections were normalized to those of White *et al.* [8], with an accuracy of 15%.

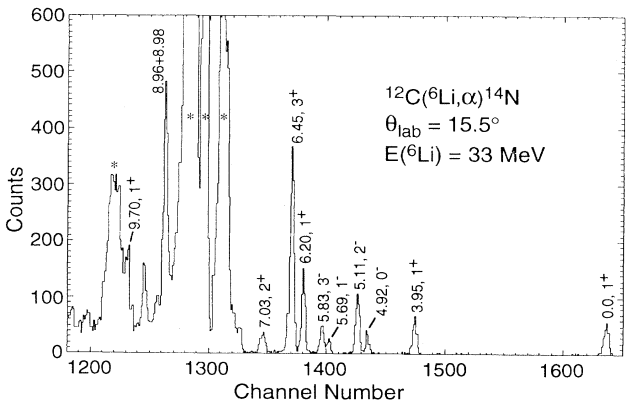

FIG. 1. Sample spectrum from the ^{12}C(^{6}Li,α)^{14}N reaction. The peaks labeled by * arise from elastic and inelastic scattering from ^{12}C and target contaminants.

The polarization observables were extracted from the data by taking appropriate combinations of the left (L) and right (R) ratios of polarized yield to unpolarized yield. With the AP as defined in the Madison convention [20], the relevant equations are

$$L - R = \sqrt{8}t_{10}iT_{11}, \tag{1}$$

and

$$L + R - 2 = 2t_{20}(-\tfrac{1}{2}T_{20} - \sqrt{\tfrac{3}{2}}T_{22}) = 2t_{20}{}^TT_{20}, \tag{2}$$

for the β=90°, ϕ=0° orientation,

$$L - 1 = R - 1 = t_{20}T_{20}, \tag{3}$$

for the β=0° orientation, and

$$L - R = \sqrt{6}t_{20}T_{21}, \tag{4}$$

for the β=45°, ϕ=90° orientation.

III. DISCUSSION OF THE DATA

The cross section and analyzing power angular distributions for all states are shown in Figs. 2–4. The T_{22} distributions were calculated from the measured $^TT_{20}$ and T_{20} distributions. Data points are joined by curves to guide the eye, and the error bars shown are purely statistical. As reported by White *et al.* [8], there was no clear spectroscopic signature in the cross section distributions. However, patterns emerged from the AP distributions that indicate the possibility of extracting ^{14}N structure information. In the vector AP, three of the 1^+ states look very similar, with the ground state oscillating out of phase with the others, and to a lesser degree this pattern is also seen in the T_{21} distributions. However, the T_{20} distributions exhibited a different grouping: the 3.95 and 6.20 MeV states, both presumed to be L = 0 in Ref. [8], look nearly identical over the whole range, while the ground state and 9.70 MeV state oscillate out of phase with the other two states. Although no clearly J-dependent patterns were found, the $^TT_{20}$ distributions seem to distinguish between natural and unnatural parity states. As can be seen in Fig. 3, the $^TT_{20}$ distributions for the 1^+ states are fairly flat, with relatively large, positive values. In fact, all unnatural parity states had positive $^TT_{20}$ analyzing powers, while the natural parity states exhibited large negative values for $^TT_{20}$, with more oscillatory distributions.

This $^TT_{20}$ effect has been seen in ($\vec{d}$,α) studies; in particular, the 16 MeV ^{36}Ar($\vec{d}$,α)^{34}Cl study of Bhat *et al.* [15] populated 1^+, 2^+, and 3^+ final states which clearly

exhibit this pattern. The effect can be explained qualitatively using the peripheral plane wave model of Santos and Eiró [21]. This model is a plane wave Born approximation for a deuteron transfer process wherein the bound state of the deuteron in the light system ($^{6}\mathrm{Li} = \alpha + d$ here) is assumed to be in a pure S-wave state. With no further approximations, the following results can be derived using standard angular momentum algebra. The tensor analyzing powers T_{2q} are proportional to spherical harmonics $Y_{2q}(\hat{Q})$, where $\hat{Q}$ is in the direction of the transferred momentum. The vector AP vanish in this model; it is a general property of plane wave approximations that k = odd AP are zero. This model leads to the following $({}^{T}T_{20})_{L,J}$ results for $J = L$, $L \pm 1$:

$$({}^{T}T_{20})_{L,L} = -\sqrt{\frac{1}{8}}, \tag{5}$$

$$({}^{T}T_{20})_{L,L+1} = \frac{L}{\sqrt{8}(2L+3)}, \tag{6}$$

$$({}^{T}T_{20})_{L,L-1} = \frac{L+1}{\sqrt{8}(2L-1)}, \tag{7}$$

in which $L(\equiv L_2$ later) is the orbital angular momentum of the deuteron in the residual nucleus of spin J.

Equation (5) is for $J = L$, which is a natural parity state, and the predicted ${}^{T}T_{20}$ is negative. Equations (6) and (7) are for the unnatural parity states, and both are positive. When L mixing is taken into account for the unnatural parity states, where $L = J \pm 1$, the simple results above are modified to include the L mixing ratio:

$$({}^{T}T_{20})_{J} = \frac{(J+2)x^2 - 6[J(J+1)]^{\frac{1}{2}}x + J - 1}{\sqrt{8}(2J+1)(1+x^2)}, \tag{8}$$

where x is proportional to the ratio $S^{\frac{1}{2}}_{J+1}/S^{\frac{1}{2}}_{J-1}$ of the cluster spectroscopic amplitudes with the proportionality depending on the angle. Note that the presence of the linear term in x makes ${}^{T}T_{20}$ sensitive to the sign of the mixing ratio. The general case including both D-state

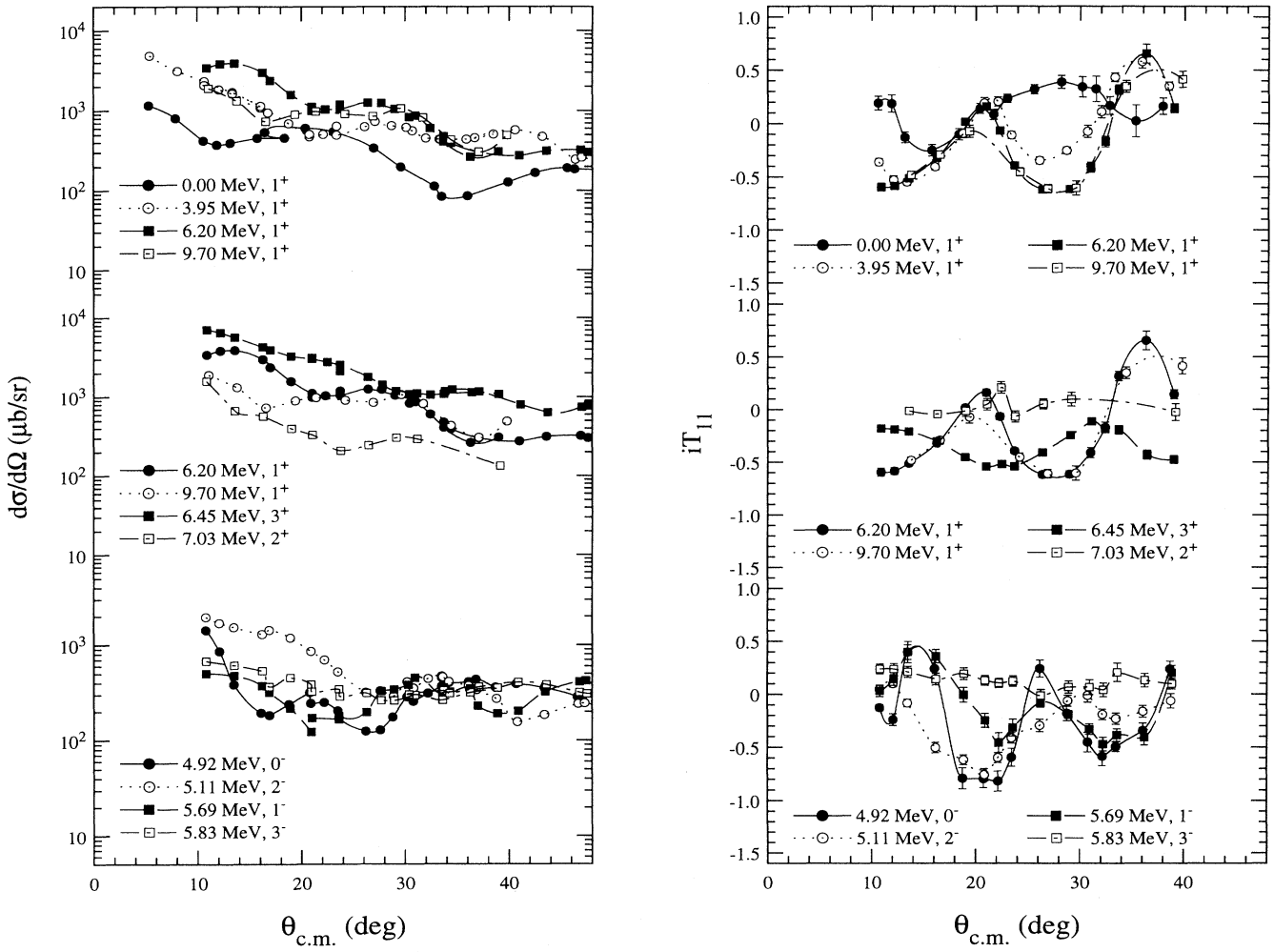

FIG. 2. Cross sections and vector analyzing powers iT_{11} for transitions to states in ^{14}N shown. Lines are drawn through the data points to guide the eye. The data for the transitions to the 6.20 and 9.70 MeV, 1^{+} states are repeated in the middle of the figure for comparison with the 6.45, 3^{+} and 7.03 MeV, 2^{+} transitions.

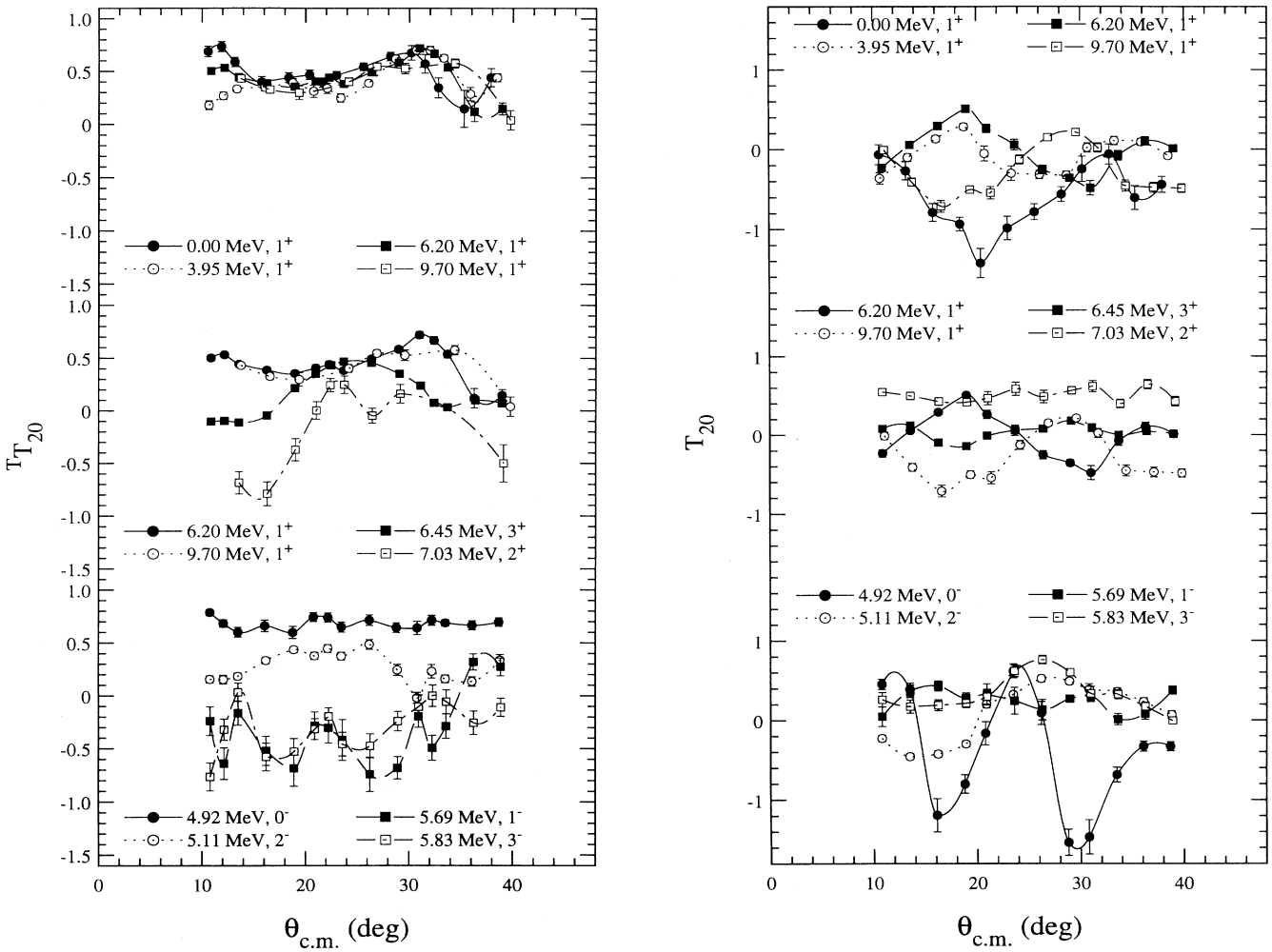

FIG. 3. Same as for Fig. 2, except that the analyzing power data ${}^{T}T_{20}$ and T_{20} are shown.

effects in ^{6}Li and final state L mixing is not addressed in this simple model.

While the above dynamical arguments are appealing at first sight, the presence of large, nonzero vector AP for essentially every state investigated brings into question the validity of the plane wave approximation. One model-independent approach is to write down general expressions for the tensor and vector analyzing powers using reaction amplitudes which are characterized by the quantum numbers L, M_L corresponding to the orbital angular momentum transferred from the initial ^{6}Li spin state to the final ^{14}N spin state. Selection rules on L and M_L are imposed only by consideration of the conservation of total angular momentum and parity and not by the reaction dynamics assumed. For the reaction of interest here $^{12}\mathrm{C}(^6\vec{\mathrm{Li}},\alpha)^{14}\mathrm{N}^*$ we will restrict our attention to final states with $J^\pi = 0^\pm, 1^\pm$; so that $L = 0, 1, 2$ for $1^\pm$ states and $L = 1$ for $0^\pm$ states. Defining amplitudes by the usual spectroscopic notation S,P,D and adding a suffix M_L (referred to the transverse frame) for each amplitude we find for ${}^{T}T_{20}$ the results:

$$0^-: \quad {}^{T}T_{20} = +\frac{1}{\sqrt{2}}, \tag{9}$$

$$0^+: \quad {}^{T}T_{20} = -\sqrt{2}, \tag{10}$$

$$1^+: \quad {}^{T}T_{20} = \frac{1}{\sqrt{2}} - \frac{\sqrt{2}|(S_0/\sqrt{2}) - D_0|^2}{|S_0|^2 + |D_0|^2 + |P_0|^2 + |D_2|^2 + |D_{-2}|^2}, \tag{11}$$

$$1^-: \quad {}^{T}T_{20} = -\frac{1}{2\sqrt{2}} - \frac{3}{\sqrt{2}} \frac{\mathrm{Re}(P_1 D_1^* - P_{-1} D_{-1}^*)}{|P_1|^2 + |P_{-1}|^2 + |D_1|^2 + |D_{-1}|^2}. \tag{12}$$

These results show a leading constant term which has

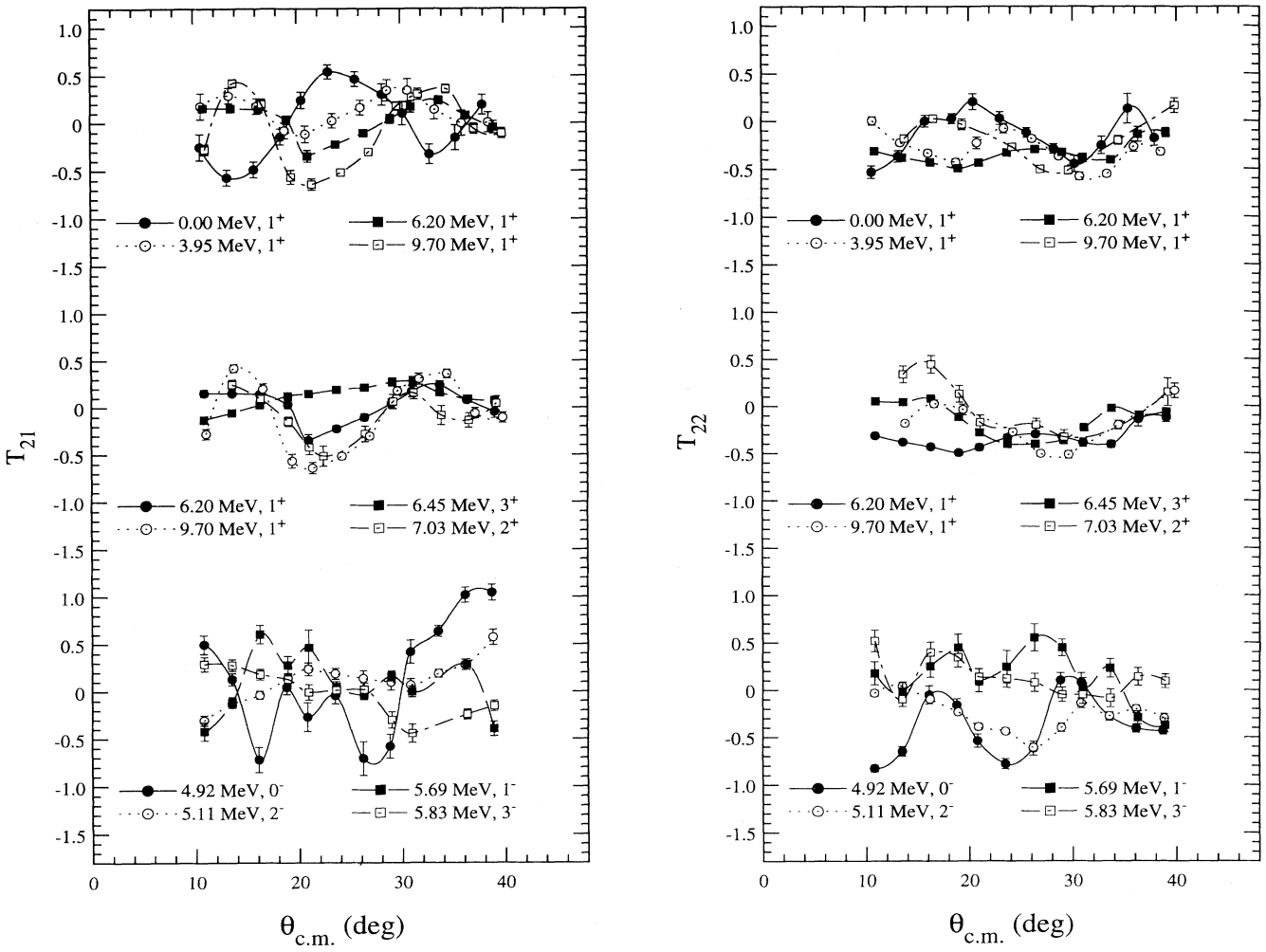

FIG. 4. Same as for Fig. 2, except that the analyzing power data T_{21} and T_{22} are shown.

the desired sign oscillation appropriate to natural and unnatural parity states in ^{14}N. The result for a transition to the 0^+ state is included for completeness, even though such a transition was not observed in the present work.

For the special case of a 0^- final state, the other observables are

$$T_{20} = \sqrt{2}(|\tilde{P}_1|^2 - |\tilde{P}_0|^2)/N_0, \tag{13}$$

$$T_{21} = \sqrt{\frac{3}{2}}(2\mathrm{Re}\tilde{P}_0\tilde{P}_1^*)/N_0, \tag{14}$$

$$T_{22} = -\sqrt{3}|\tilde{P}_1|^2/N_0, \tag{15}$$

$$iT_{11} = -\sqrt{\frac{3}{2}}(2\mathrm{Im}\tilde{P}_0\tilde{P}_1^*)/N_0, \tag{16}$$

where M_L is referred to the Madison frame, the notation $\tilde{P}_{M_L}$ is used to distinguish amplitudes referred to the Madison frame from the P_{M_L} transverse frame amplitudes, and $N_0 = 2|\tilde{P}_1|^2 + |\tilde{P}_0|^2$. The above shows that $T_{21} = iT_{11} = 0$ whenever T_{20} is a maximum $(+\frac{1}{\sqrt{2}})$ or a minimum $(-\sqrt{2})$ corresponding to $|\tilde{P}_0| = 0$ or $|\tilde{P}_1| = 0$, respectively. Note that T_{22} is always negative, with a minimum value of $-\frac{\sqrt{3}}{2}$ and a maximum of zero. These general rules are exhibited by the data for the 0^- state, which exhibits a maximum (minimum) in T_{20} near 24° (30°) and a T_{22} distribution which is negative over the entire angular range measured. Near 24°, both iT_{11} and T_{21} are close to zero, as is T_{21} near 30°. It appears that iT_{11} is small, but negative near 30°; however, since the AP oscillate rapidly here, and since for the 0^- state they are related by

$$iT_{11}^2 + \tfrac{1}{2}T_{20}^2 + T_{21}^2 + T_{22}^2 = 1, \tag{17}$$

near an extreme value of T_{20}, iT_{11} can be small, but nonzero. Therefore, the data are consistent with the general rules at 30° as well.

The corresponding results for the 1^+ states are

$$T_{20} = \left[2\mathrm{Re}\left(\tilde{S}_0\tilde{D}_0^* - \frac{3}{\sqrt{2}}\tilde{P}_1\tilde{D}_1^*\right) + \frac{1}{\sqrt{2}}(2|\tilde{D}_2|^2 - |\tilde{P}_1|^2 - |\tilde{D}_1|^2 - |\tilde{D}_0|^2)\right] \Big/ N_1, \tag{18}$$

$$T_{21} = -\left[2\mathrm{Re}\left(\tilde{S}_0\tilde{D}_1^* + \frac{3}{2\sqrt{2}}\tilde{D}_0\tilde{P}_1^* - \frac{\sqrt{3}}{2}(\tilde{D}_1\tilde{D}_2^* + \tilde{P}_1\tilde{D}_2^*) - \frac{1}{2\sqrt{2}}\tilde{D}_0\tilde{D}_1^*\right)\right] \Big/ N_1, \tag{19}$$

$$T_{22} = \left[2\mathrm{Re}\left(\tilde{S}_0\tilde{D}_2^* + \frac{\sqrt{3}}{2}\tilde{P}_1\tilde{D}_1^* + \frac{1}{\sqrt{2}}\tilde{D}_0\tilde{D}_2^*\right) - \frac{\sqrt{3}}{2}(|\tilde{P}_1|^2 + |\tilde{D}_1|^2)\right] \Big/ N_1, \tag{20}$$

$$iT_{11} = -\left[2\mathrm{Im}\left(\tilde{S}_0\tilde{P}_1^* + \frac{1}{2\sqrt{2}}(\tilde{P}_1\tilde{D}_0^*) + \frac{\sqrt{3}}{2}(\tilde{P}_1\tilde{D}_2^* + \tilde{D}_1\tilde{D}_2^*) + \frac{3}{2\sqrt{2}}(\tilde{D}_0\tilde{D}_1^*)\right)\right] \Big/ N_1, \tag{21}$$

with

$$N_1 = |\tilde{S}_0|^2 + |\tilde{D}_0|^2 + 2(|\tilde{P}_1|^2 + |\tilde{D}_1|^2 + |\tilde{D}_2|^2). \tag{22}$$

These are relatively complicated, but we do note that T_{22} has negative noninterfering terms so that its average value should be negative as observed in Fig. 4. The noninterfering terms in T_{20} are positive when $|M_2|$=2 and negative for $|M_2|$=1,0, and no conclusions can be drawn unless one resorts to specific dynamics. Both T_{21} and iT_{11} involve only interfering amplitudes so that both sign values are expected and observed.

IV. DWBA ANALYSIS

A. Nilsson model description of ^{14}N

The literature is rich with proposed structure models for the nucleus ^{14}N. These models can be divided into two broad categories, as discussed by Amos *et al.* [22]. The first is one in which the wave functions are determined by specifying a Hamiltonian for light nuclei and then fine tuning it to reproduce the observed spectra and static moments. The Cohen-Kurath (C-K) [23] model calculations are the standard for this class. The second class comprises phenomenological wave functions specified by selecting a general, parametrized form and then determining the strength coefficients, subject to a normalization constraint, by fitting a particular set of static and dynamic observables. Typical of these are the wave functions of Huffman *et al.* [24], which were generated by fitting electron scattering form factors, the static magnetic moment of ^{14}N, the radiative lifetime of the J^π, $T = 0^+$, 1 state at 2.313 MeV (which forms an isospin triplet with the ground states of ^{14}C and ^{14}O), and the ^{14}C$(\beta^-)^{14}$N Gamow-Teller (G-T) strength.

Although both classes of wave function have been used with varying degrees of success, there are a number of difficulties with each of them. For example, the standard problem with the C-K wave functions is their inability to describe the electron scattering data as discussed in Ref. [24]. However, as is pointed out by Talmi [25], the phenomenological wave functions of Ref. [24], in addition to failing to yield the anomalously slow decay rate of ^{14}C, are eigenstates of a shell-model Hamiltonian which gives the spin-orbit interaction the opposite sign compared to the standard Mayer-Jensen shell model. As regards the ^{14}C decay rate, the required "accidental" cancellation of the G-T matrix element could be obtained within the p^{-2} configuration by the inclusion of a tensor force [26], or it could also be generated by configuration mixing [27]. In a comment on the paper of Amos *et al.* [22], Bennhold and Tiator [28] conclude that what is needed is to repeat the C-K calculations, taking into account all of the information on dynamical observables that has been obtained over the past 20 years and including configurations outside the 1p shell.

Since the description of the states observed in this work requires configurations in both the p shell and the sd shell, rather than undertaking the formidable task of expanding the model space to generate more realistic shell-model wave functions, a different approach was chosen. The Nilsson model has long been employed successfully to account for most of the observed features of single-particle levels in hundreds of deformed nuclei. Although the best known examples are in the rare earths (A from ~150 to ~190) with typical deformations of $\beta \sim \epsilon \sim \delta \sim 0.3$, it is well known that very large ground state deformations can be found in the light nuclei. Relevant to this discussion is the deformation of ^{12}C, with $\beta \sim -0.6$, determined, e.g., by proton inelastic scattering to the 2^+ first excited state [29].

The Nilsson model provides a simple picture of the low-lying ^{14}N states; using a closed shell ^{12}C core, a single nucleon is added to produce the low-lying spectra of ^{13}C and ^{13}N. At a deformation of about -0.6 (the approximate value for ^{12}C) the four levels ($\frac{1}{2}^-$, $\frac{5}{2}^+$, $\frac{1}{2}^+$, $\frac{3}{2}^+$) above the ^{12}C core are nearly degenerate. The first few states in the ^{13}C, ^{13}N spectra are $\frac{1}{2}^-$, $\frac{1}{2}^+$, $\frac{3}{2}^-$, $\frac{5}{2}^+$. The $\frac{3}{2}^-$ state is a rotational excitation in the $K = \frac{1}{2}^-$ band, and when corrections are applied for the rotational energy of the levels, the correct ordering is obtained using

TABLE I. Proposed ^{14}N configurations. Here (Ω_1,Ω_2) refer to the Nilsson orbitals into which the transferred nucleons are placed to form the given state in ^{14}N.

		"Dominant configurations"	
E_x(MeV),J^π	(Ω_1,Ω_2)	This work	Ref. [34]
0.00(g.s.),1^+	$(\frac{1}{2}^-,\frac{1}{2}^-)$	$(p_{\frac{1}{2}})^2$	$(p_{\frac{1}{2}})^2$
3.95, 1^+	$(\frac{1}{2}^+,\frac{1}{2}^+)$	$(s_{\frac{1}{2}})^2$	core excited
4.92, 0^-	$(\frac{1}{2}^-,-\frac{1}{2}^+)$	$p_{\frac{1}{2}}-s_{\frac{1}{2}}$	$p_{\frac{1}{2}}-s_{\frac{1}{2}}$
5.11,2^-	$(\frac{5}{2}^+,-\frac{1}{2}^-)$	$p_{\frac{1}{2}}-d_{\frac{5}{2}}, p_{\frac{3}{2}}-d_{\frac{5}{2}}$	$p_{\frac{1}{2}}-d_{\frac{5}{2}}$
5.69,1^-	$(\frac{1}{2}^-,\frac{1}{2}^+)$	$p_{\frac{1}{2}}-s_{\frac{1}{2}}$	$p_{\frac{1}{2}}-s_{\frac{1}{2}}$
5.83,3^-	$(\frac{5}{2}^+,\frac{1}{2}^-)$	$p_{\frac{1}{2}}-d_{\frac{5}{2}}$	$p_{\frac{1}{2}}-d_{\frac{5}{2}}$
6.20,1^+	$(\frac{5}{2}^+,-\frac{3}{2}^+)$	$d_{\frac{5}{2}}-d_{\frac{3}{2}}, (d_{\frac{5}{2}})^2$	$(s_{\frac{1}{2}})^2$
6.45,3^+	$(\frac{5}{2}^+,\frac{1}{2}^+)$	$s_{\frac{1}{2}}-d_{\frac{5}{2}}$	$s_{\frac{1}{2}}-d_{\frac{5}{2}}$
7.03,2^+	$(\frac{5}{2}^+,-\frac{1}{2}^+)$	$s_{\frac{1}{2}}-d_{\frac{5}{2}}$	core excited
9.70,1^+	$(\frac{3}{2}^+,-\frac{1}{2}^+)$	$(s_{\frac{1}{2}})^2$	$(d_{\frac{5}{2}})^2$

the sequence $\frac{1}{2}^-$, $\frac{5}{2}^+$, $\frac{1}{2}^+$, $\frac{3}{2}^+$ given above. Since the slope of the $\frac{1}{2}^-$ orbit is negative for oblate (negative) deformations, one expects the deformation of the ^{13}C, ^{13}N ground states to be somewhat less than the ^{12}C deformation, and that of the ^{14}N ground state, formed by adding a second nucleon to this orbit, to be smaller still. This is what is observed experimentally, e.g., see Ref. [29], with reported β_2 values of $-(0.41\rightarrow0.47)$ for ^{13}C and ~ -0.25 for ^{14}N.

By placing the two valence nucleons in ^{14}N into the four lowest available Nilsson orbitals, the entire low-lying spectrum can be generated. Table I shows the proposed Nilsson model configurations for the states of interest. For the 1^+ states, which are the primary focus of this analysis, the ground state configuration is p^2, while the other three 1^+ states are built from configurations in the *sd* shell. This gives an extra radial node in both L=0 and L=2 components as compared with the ground state. This grouping suggests a possible source for the phase shift between the ground state and the other three 1^+ states seen in the iT_{11} angular distributions.

B. Spectroscopic amplitudes for ^{14}N=*d*+^{12}C

In the previous section, a simple, qualitative description of ^{14}N in terms of the Nilsson model was presented. In this section, we expand on this discussion, building wave functions for ^{14}N and calculating the spectroscopic factors for the Nilsson model deuteron transfer.

In the following discussion, the reaction $A(a,b)B$ will be described using the cluster transfer notation $A+a(=b+d)\rightarrow B(=A+d)+b$, in which A is the target, ^{12}C, a is the projectile, ^6Li, comprising a $b(=\alpha)$+d cluster, and d is the transferred deuteron. We assume the deuteron to be a nodeless (l_{np}=0) s-wave state with $I_d = I_a$=1. Since I_A=0, the spin of the ^{14}N state is $\vec{J}_B = \vec{I}_d + \vec{L}_2$, so that for the positive (negative) parity states $\vec{L}_2$ is even (odd). Further, $\vec{L}_2$ can have at most two values in the range $0 \leq \vec{L}_2 \leq 4$ for the low-lying states. In particular, the 1^+ states have $\vec{L}_2$=0, 2 only.

Configurations built from $(1p)^2$ and *sd* shell configurations built from $(1d)^2$, $(2s)^2$, and $(2s,1d)$ will occur for the 1^+ states. In this work, the principal quantum numbers n_p, n_n, N_2 begin at zero, so in conforming to the usual spectroscopic notation for harmonic oscillator wave functions n+1 is used, e.g., the $1p$ shell has n=0. Conservation of energy for oscillators requires $2N_2+L_2 = 2n_p+l_p+2n_n+l_n$ assuming $n=l_{np}=0$ for an s-wave deuteron. For the $(1p)^2$ configurations, the required values are (N_2,L_2)=(1,0) and (0,2), i.e., we have $2S$ and $1D$ components in the d-^{12}C wave function. For the *sd* shell configurations, these requirements yield $3S$ and $2D$ components, i.e., these states yield an extra node in the d-^{12}C wave functions. All of the observed states have $0 \leq L_2 \leq 4$ and $0 \leq N_2 \leq 2$.

The calculated spectroscopic amplitudes for the low-lying states in ^{14}N are shown in Table II, grouped according to parity and $2N_2+L_2$ value. Spectroscopic factors for ^6Li were taken from Werby *et al.* [30], who deduced values of S_0=0.69 and S_2=0.04 from angular distribution measurements of $^6Li(p,^3He)^4He$. Their measurements were not sensitive to the signs of the spectroscopic amplitudes; the relative signs, as well as the magnitude of the amplitudes, were tested in the present work, as described in the next section. It will be convenient for this discussion to define here the L mixing ratio $R_{LL'} \equiv S_L^{\frac{1}{2}}/S_{L'}^{\frac{1}{2}}$ and include it in Table II.

C. DWBA calculations

Exact finite-range deuteron cluster transfer (FRDCT) DWBA calculations were performed for the positive parity states using the computer code DWUCK5 [31]. The negative parity states have cross-shell configurations and are therefore less suitable for the deuteron cluster trans-

TABLE II. Spectroscopic amplitudes for the low-lying states in ^{14}N. The L mixing ratio has been defined as $R_{LL'} = S_L^{\frac{1}{2}}/S_{L'}^{\frac{1}{2}}$.

E_x(MeV), J^π	$(\Omega_1^\pi,\Omega_2^\pi)$	$2N+L$	$S_0^{\frac{1}{2}}$	$S_2^{\frac{1}{2}}$	R_{20}
0.00, 1^+	$(\frac{1}{2}^-,\frac{1}{2}^-)$	2	−0.279	+0.317	−1.136
3.95, 1^+	$(\frac{1}{2}^+,\frac{1}{2}^+)$	4	+0.265	+0.0290	+0.109
6.20, 1^+	$(\frac{5}{2}^+,-\frac{3}{2}^+)$	4	+0.217	+0.0070	+0.032
9.70, 1^+	$(\frac{3}{2}^+,-\frac{1}{2}^+)$	4	−0.0191	+0.259	−13.6
E_x(MeV), J^π	$(\Omega_1^\pi,\Omega_2^\pi)$	$2N+L$	$S_2^{\frac{1}{2}}$	$S_4^{\frac{1}{2}}$	R_{42}
6.45, 3^+	$(\frac{5}{2}^+,\frac{1}{2}^+)$	4	+0.291	−0.0026	−0.009
7.03, 2^+	$(\frac{5}{2}^+,-\frac{1}{2}^+)$	4	+0.176	—	0
E_x(MeV), J^π	$(\Omega_1^\pi,\Omega_2^\pi)$	$2N+L$	$S_1^{\frac{1}{2}}$	$S_3^{\frac{1}{2}}$	R_{31}
4.92, 0^-	$(\frac{1}{2}^-,-\frac{1}{2}^+)$	3	+0.350	—	0
5.11, 2^-	$(\frac{5}{2}^+,-\frac{1}{2}^-)$	3	−0.068	+0.113	−1.66
5.69, 1^-	$(\frac{1}{2}^-,\frac{1}{2}^+)$	3	+0.118	—	0
5.83, 3^-	$(\frac{5}{2}^+,-\frac{1}{2}^+)$	3	—	+0.215	∞

TABLE III. Bound state parameters. Radii have the form $R = r_0 A_T^{\frac{1}{3}}$, and λ is the usual Thomas-Fermi spin-orbit parameter, giving the strength of the spin-orbit relative to the central potential.

Nucleus	r_0(fm)	a(fm)	λ	r_{0C}(fm)
^{14}N	1.94	0.65	25	1.73
^{6}Li	2.15	0.65	25	1.73

fer. For the positive parity calculations, the ^{14}N states were assumed to be formed from a deuteron bound to a closed shell ^{12}C core, with the deuteron in an internal $1s$ state. Both $2s$ and $1d$ components were included in the relative motion of the α particle and the deuteron in ^{6}Li using the spectroscopic factors of Werby *et al.* [30]. Woods-Saxon bound state parameters, shown in Table III, were obtained from Ref. [8]. The bound state form factors were generated by searching on the potential well depth until the known deuteron separation energy was obtained, using the sign convention that the form factors are positive at infinity.

The Woods-Saxon optical model parameters are shown in Table IV. Those for entrance channel distorted waves were taken from the 30 MeV ^{6}Li + ^{12}C elastic scattering data analysis of Reber *et al.* [32]. The optical model parameters for the exit channel distorted waves were taken from the analysis of 30 MeV ^{14}N + α elastic scattering by Lowe and Barnett [33], which were also used by White *et al.* [8].

Calculations for the 1^+ states are shown in Figs. 5 and 6, demonstrating the effect of the various L mixings. The angular momentum L_1 refers to ^{6}Li and L_2 to ^{14}N. In these plots, the solid line is a purely L_1=L_2=0 calculation, the dotted line is for L_1=0 in ^{6}Li and L_2=2 in ^{14}N, the dashed line is for L_1=0 in ^{6}Li and both L_2=0 and L_2=2 in ^{14}N using the Nilsson spectroscopic amplitudes from Table II, and the dot-dashed line is the full calculation including L_i mixing in both ^{6}Li and ^{14}N. The choice of a positive sign for the ^{6}Li L_1 mixing ratio provided a better fit to the entire data set.

The descriptions of the cross sections, shown in Fig. 5, are fairly reasonable. The two predominantly L_2=0 states, 3.95 MeV and 6.20 MeV, were fit quite well at the forward angles. As expected, the dotted line (pure L_2=2 in ^{14}N) gave the poorest fit to these two states. However, the cross sections do not seem particularly sensitive to L_i mixing, in fact, they are hard pressed to distinguish between pure L_2=0 and pure L_2=2.

The vector AP, shown in Fig. 5 is much more sensitive to L mixing. The purely L_1=L_2=0 calculation (solid line) generated almost no iT_{11}, even though a reasonable spin-orbit potential was included in the entrance channel, as well as in the bound states. The full calculation (dot-dashed line) is required to reproduce adequately the structure in the ground state distribution, suggesting that iT_{11} is sensitive to the presence of L_1=2 and L_2=2 amplitudes. Unfortunately, the other three 1^+ states could not be reproduced by the calculations, which show effects due to Q value and binding energy that are not present in the data. For the 3.95 MeV and 6.20 MeV states, the solid and dashed lines overlap, while for the 9.70 MeV state, the dotted and dashed lines overlap.

The TAP, shown in Fig. 6, exhibit similar ambiguities, but they clearly show the presence of L_i=2 components in the transfer. The best description of the data is seen in the ${}^{T}T_{20}$ calculations. The full calculation (dot-dashed line) gives the best fit for all except the 6.20 MeV state, and in this case the full calculation does predict the correct sign and only slightly underpredicts the magnitude. The 9.70 MeV calculation is clear evidence that ${}^{T}T_{20}$ cannot distinguish between the L_1=2 component in ^{6}Li and L_2=2 in ^{14}N. The calculations do follow the observed rule that ${}^{T}T_{20}$ should be positive for unnatural parity states.

The T_{20} results are quite poor, only vaguely following the trends in the data. As in the ${}^{T}T_{20}$ calculations, nonzero results could be obtained only when L_i=2 components were present. Both the data and the calculations look similar for the 3.95 and 6.20 MeV states, but beyond that little can be said. The interference effect in the 9.70 MeV calculations is interesting. Without the ^{6}Li L_1=2 component (dashed curve), the calculation follows the data reasonably well. Adding this component spoils the fit, leaving open the possible conclusion that there is a relative sign problem between the L_1=2 and L_2=2 spectroscopic amplitudes for this transition.

For the T_{21} results, the 9.70 MeV calculations show the interference between the two L_i=2 components, which worsens the fit. In the other three cases, the full calculations follow the data reasonably well.

The next set of calculations, shown in Fig. 7, are aimed at resolving the questions raised above about the relative signs of the spectroscopic amplitudes. In these plots, the signs of the L_i mixing ratios are as follows: the solid line has $R_{20}(^{14}\mathrm{N})$ negative and $R_{20}(^{6}\mathrm{Li})$ positive, the dotted line has both ratios negative, the dashed line has both positive, and the dot-dashed line has ^{14}N positive and ^{6}Li negative. Since the g.s. is predicted to have roughly equal L_2=0,2 amplitudes ($|R_{20}|$=1.14), it should be sensitive to the sign of both $R_{20}(^{6}\mathrm{Li})$ and $R_{20}(^{14}\mathrm{N})$. The cross section favors the dashed line, based on coming closest to placing correctly the first minimum, although the dotted curve is very nearly the same. The preference for these two

TABLE IV. Woods-Saxon optical model parameters for ^{12}C(^{6}Li,^{6}Li)^{12}C and ^{14}N(α,α)^{14}N elastic scattering.

	U_R (MeV)	r_R (fm)	a_R (fm)	W_{vol} (MeV)	r_I (fm)	a_I (fm)	V_{LS} (MeV)	r_{LS} (fm)	a_{LS} (fm)	r_c (fm)
^{6}Li+^{12}C	244	1.15	0.78	10.0	2.20	0.78	3.6	1.20	0.65	2.24
α+^{14}N	187.4	1.268	0.625	28.76	1.539	0.145	...	...	...	1.30

sign choices is echoed even more convincingly in the iT_{11} plot. Here also, the sensitivity seems to be to the relative sign between the mixing ratios, rather than to the sign of either R_{20}, i.e., iT_{11} shows a preference for the two ratios having the same signs. The TAP are more sensitive to the signs of the individual ratios. All three of the TAP show significant changes in both the magnitude and the phase of the oscillations, which depend on which sign(s) get(s) changed. None of the calculations reproduced the T_{20} data, but the solid line follows the trends in T_{21} and ${}^{T}T_{20}$ reasonably well. The dashed line is not much worse for these two TAP. So, while all of the g.s. data seem to prefer $R_{20}(^{6}\mathrm{Li})>0$, the results are ambiguous for the sign of $R_{20}(^{14}\mathrm{N})$. The TAP prefer the negative sign, in agreement with the Nilsson model prediction, and the cross section and iT_{11} prefer the positive sign.

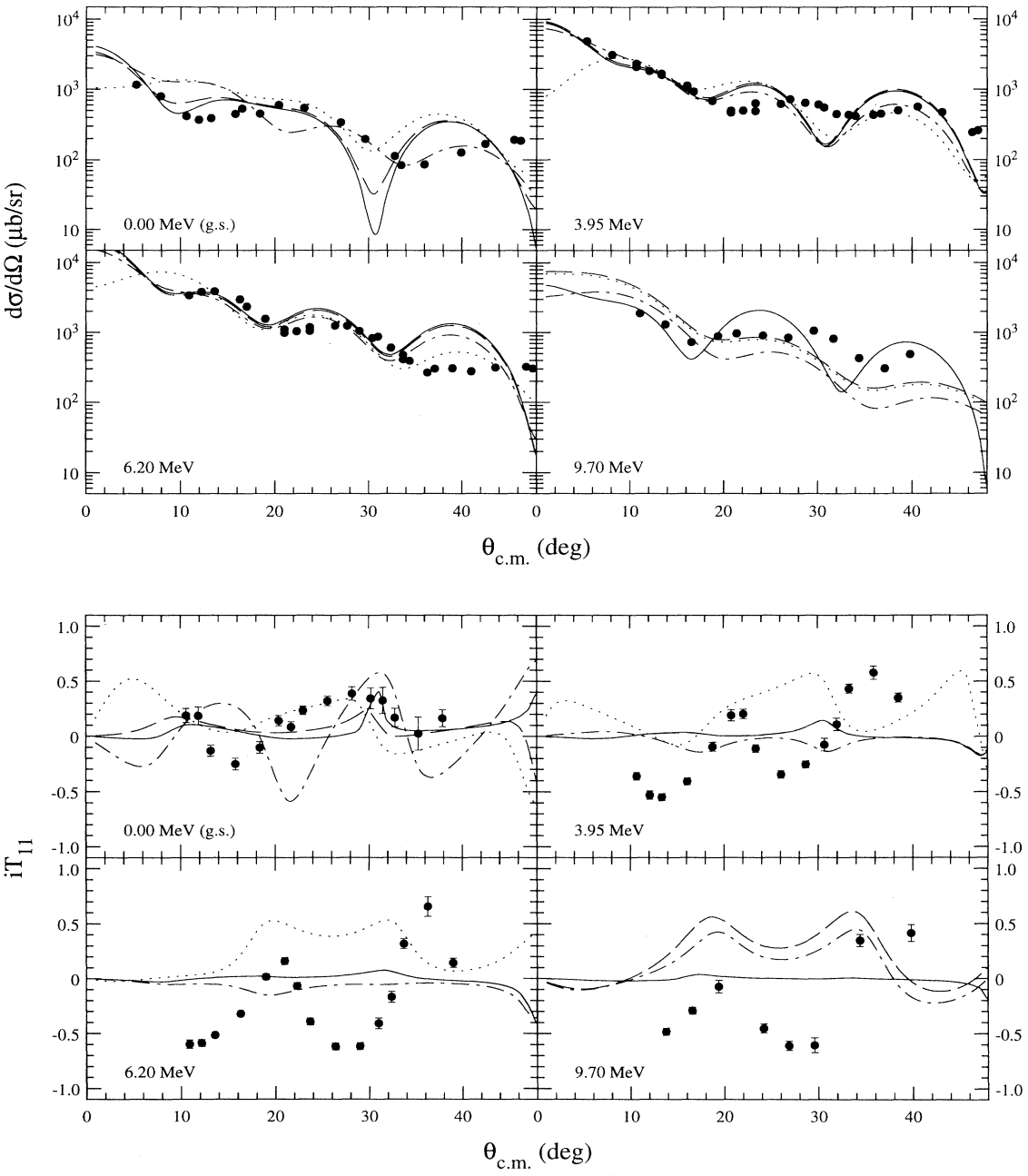

FIG. 5. FRDCT-DWBA cross section and iT_{11} calculations for transitions to the 1^{+} state. The solid line is for $L_1=0$ deuteron transfer from ^{6}Li to an $L_2=0$ orbit in ^{14}N. The dotted line is for $L_1=0$ in ^{6}Li and $L_2=2$ in ^{14}N. The dashed line is for $L_1=0$ in ^{6}Li and mixed $L_2=0,2$ in ^{14}N using the spectroscopic amplitudes of Table II. The dot-dashed line is the full calculation that includes L mixing in both ^{6}Li and ^{14}N. In the iT_{11} figure, the solid and dashed lines overlap for the 3.95 and 6.20 MeV states while for the 9.70 MeV state, the dotted and dashed lines overlap.

The effect of changing the sign of $R_{20}(^6\mathrm{Li})$ in the 3.95 MeV calculation is shown in Fig. 8. For simplicity, the calculation shown has $R_{20}(^{14}\mathrm{N})=0$ (the predicted value is 0.11). The AP clearly prefer the solid line, which is the positive ratio, in agreement with the prediction. Similar results were seen in the 6.20 MeV calculation (not shown). However, the calculation for the 9.70 MeV state, shown in Fig. 9, yielded different results. Here large effects are seen in T_{20} and T_{21}. The fit to the T_{21} distribution is much improved by making $R_{20}(^6\mathrm{Li})<0$, shown by the dashed line. Although the two calculations for T_{20} are quite different, neither of them bears any resemblance to the data. Changing the sign had only a minor effect on the other AP and the cross section (not shown).

Calculations for the 3^+, 6.45 MeV and 2^+, 7.03 MeV states were also carried out. However, the degree of success in reproducing the data is similar to that for the just discussed 1^+ states and the detailed results are not

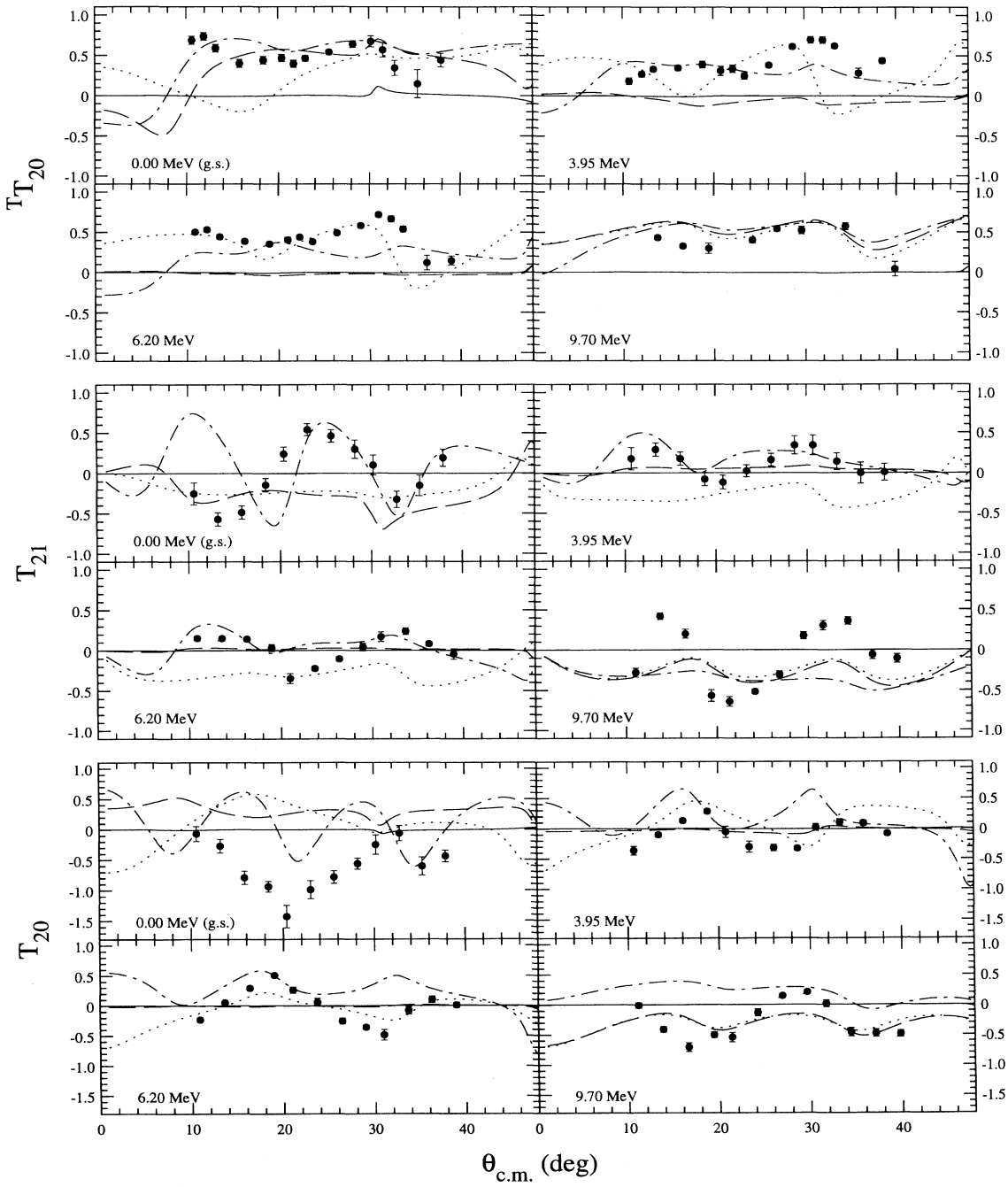

FIG. 6. Same as for Fig. 5, except that the $^TT_{20}$, T_{21}, and T_{20} data and calculations are shown.

presented here.

The assumptions implicit in analyzing the data in the present work are that the transitions are moderately strong and proceed by a one-step deuteron cluster transfer. One indication of the validity of these assumptions is the cross section normalization factors. The cross section calculated by DWUCK5 is related to the experimental cross section by

$$\left(\frac{d\sigma}{d\Omega}\right)_{\rm exp} = N\left[\frac{2J_f+1}{2J_i+1}\left(\frac{d\sigma}{d\Omega}\right)_{\rm DWUCK}\right], \qquad (23)$$

where N is the normalization factor, which was chosen to best match the forward angle maxima. In Table V, the normalization factors are shown for the calculations which included ^{6}Li S- and D-state contributions and all allowed L values in ^{14}N with the Nilsson model spectroscopic amplitudes. These are compared with the normalization factors from White *et al.* [8], using True's [34] wave functions ($N_{\rm T}$) and the Cohen-Kurath wave functions ($N_{\rm CK}$). In all cases, the calculations underpredict the cross sections somewhat. However, the full finite-range calculations including the L_2 mixing effects and the ^{6}Li D state did provide noticeable improvement to the cross section fits for most of the states, as compared to White's single L-transfer FRDCT calculations, and all of the normalization factors are smaller.

V. CONCLUSIONS

In the present work the first complete set of analyzing power measurements for the $(^{6}\vec{L}i,\alpha)$ reaction is presented. General rules that limit the range of allowed values for the tensor analyzing powers have been presented for $0^{\pm}$, $1^{\pm}$ final states that only require conservation of total angular momentum and parity in their derivation.

The FRDCT-DWBA calculations were somewhat successful at describing the entire data set. The AP calcu-

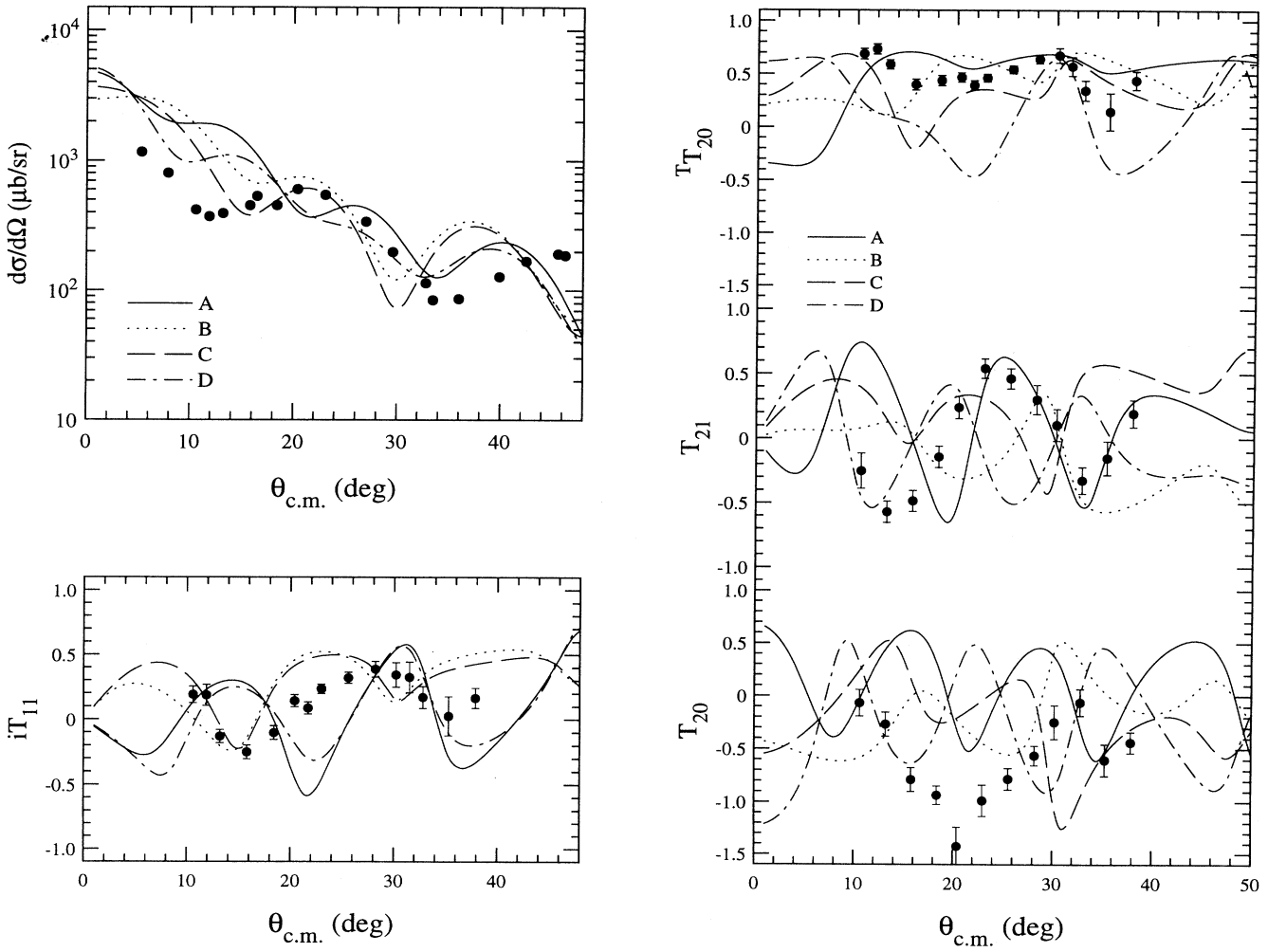

FIG. 7. Calculations showing the influence of the relative sign between the L_i=0 and L_i=2 amplitude on the observables. Curves A have the ratio R_{20} in ^{14}N negative and R_{20} in ^{6}Li positive. Curves B have both ratios negative. Curves C have both ratios positive and curves D have ^{14}N positive and ^{6}Li negative.

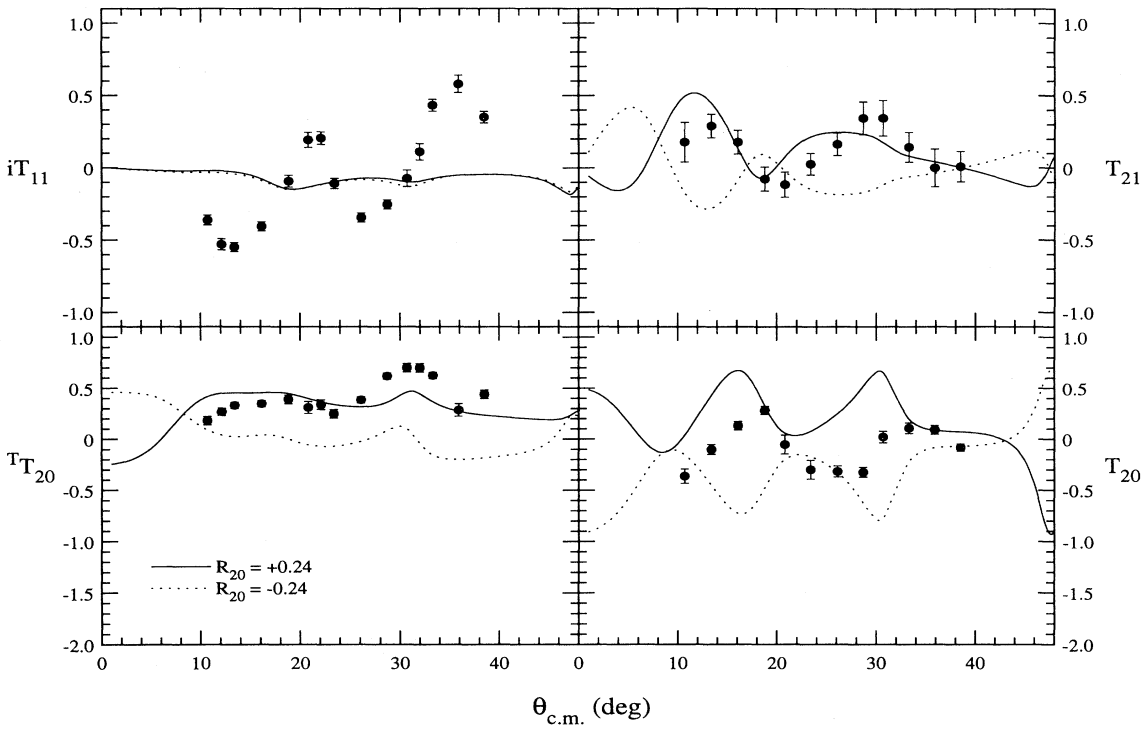

FIG. 8. Influence of the sign of R_{20} in ^{6}Li to the calculation of the transfer to the 3.95 MeV, 1^{+} state in ^{14}N. It is assumed that the d cluster is transferred into an L_2=0 orbit in ^{14}N.

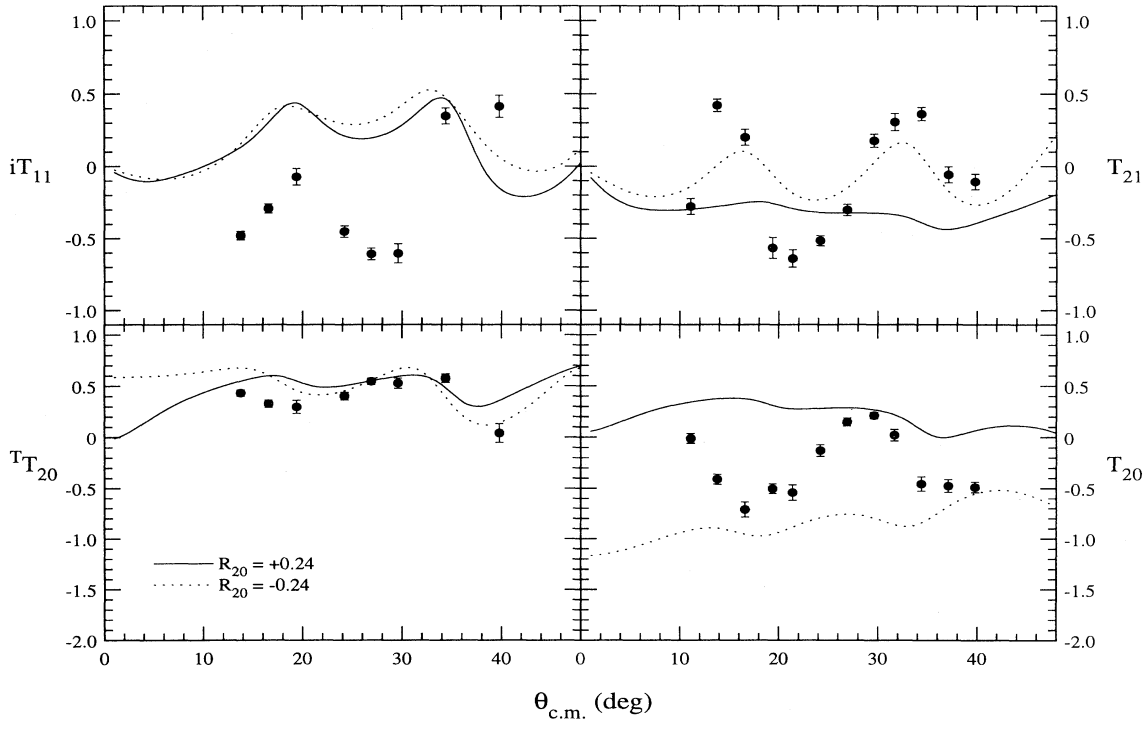

FIG. 9. Same as for Fig. 8, but for the 9.70 MeV, 1^{+} state in ^{14}N.

TABLE V. Cross section normalization factors from the present work using Nilsson wave functions (N) compared with those of White *et al.* using the wave functions of True (N_T) and Cohen-Kurath (N_{CK}).

State:	0.00	3.95	4.92	5.11	5.69	5.83	6.20	6.45	7.03	9.70
(E_x,J^π)	1^+	1^+	0^-	2^-	1^-	3^-	1^+	3^+	2^+	1^+
N	2	5	2.6	20	20	10	13	4.3	2.1	4
N_T	301	...	94	90	42	130	52	201	...	...
N_{CK}	654	1554	...	...	...	...	...	...	...	...

lations generally followed the data in most cases when the L_2 mixing and D-state effects in ^{6}Li were included. The presence of L_1=2 and L_2=2 amplitudes was seen to have significant effects on the vector analyzing powers, while the TAP seemed more sensitive just to either the L_2=2 amplitude or the D state of ^{6}Li. Because the L_i mixing was done coherently, all the AP were sensitive to both the magnitudes and the signs of the spectroscopic amplitudes. The cross section exhibited somewhat less sensitivity, although it was enough to show a clear sign preference in most cases.

The dependence on the L_i mixing ratios was tested by varying them over reasonable ranges. The sign of $R_{20}(^6\text{Li})$ was determined to be positive, judging from the whole data set. The descriptions of the data set were generally seen to improve somewhat by increasing the amount of ^{6}Li D state slightly. Values for R_{20} between 0.3 and 0.4 (the Werby value is 0.24) seemed to give the best fit when using the calculated Nilsson model spectroscopic amplitudes for ^{14}N. However, in the case of the unnatural parity states, similar effects were seen from adjusting the ^{14}N mixing ratios. These were also varied over reasonable ranges as a test of the proposed configurations. Of the stronger transitions, the 9.70 MeV, 1^+ state was the least well represented by the calculations. In particular, this transition seemed to indicate a negative $R_{20}(^6\text{Li})$ value, contradicting the remainder of data. This is fairly good evidence that the 9.70 MeV state is not given by the proposed configuration. On the other hand, the ground state is fairly well described by the calculations using the proposed configuration, except for some ambiguity as to the sign of the L_2 mixing ratio. The two predominantly L_2=0 states at 3.95 MeV and 6.20 MeV were also quite well described, except that the calculated vector analyzing power distributions are flat, while the data exhibit large oscillations. Increasing the mixing ratio did begin to generate some oscillations in the calculation, but the greatest effect seemed to be from the binding energy and Q value. These affected the calculations much more strongly than indicated by the data.

A natural next step in the analysis of the data presented here is to modify the optical model parameters or to consider the influence of projectile excitation on the $(^6\vec{Li},\alpha)$ analyzing powers. By making the optical potentials less absorbing, the periodicity of the calculated AP angular distributions could be lengthened, improving the phase-matching with the data. However, such modifications yield optical potentials which poorly describe the elastic scattering. It is known [35] that virtual excitation of ^{6}Li can produce elastic vector analyzing powers and also can influence analyzing powers for the $(\vec{d},^6\text{Li})$ reaction [36]. However, because the inclusion of channel coupling did not improve the description of the $(\vec{d},^6\text{Li})$ analyzing powers, coupled channels Born approximation calculations were not pursued here. Another reason they were not pursued is that a recent coupled channels analysis of $^{12}C(^6\vec{Li},^6Li)$ analyzing power data [37] has shown that the inelastic analyzing powers cannot be reproduced by our present knowledge of the scattering process.

This work was supported by the National Science Foundation, the U.S. Department of Energy, and the State of Florida.

[1] Pham-Dinh-Lien and L. Marquez, Nucl. Phys. **33**, 202 (1962).
[2] J.M. Blair and R.K. Hobbie, Phys. Rev. **128**, 2282 (1962).
[3] R.K. Hobbie and F.F. Forbes, Phys. Rev. **126**, 2137 (1962).
[4] S. Bashkin, V.P. Hart, and W.A. Seale, Phys. Rev. **129**, 1750 (1963).
[5] D.W. Heikkinen, Phys. Rev. **141**, 1007 (1966).
[6] C. Bergman and R.K. Hobbie, Phys. Rev. **142**, 575 (1966).
[7] R.R. Carlson and D.W. Heikkinen, Phys. Lett. **17**, 305 (1965).
[8] R.L. White, L.A. Charlton, and K.W. Kemper, Phys. Rev. C **12**, 1918 (1975).
[9] R.L. White, K.W. Kemper, L.A. Charlton, and W.J. Courtney, Phys. Rev. Lett. **31**, 254 (1973).
[10] K. Meier-Ewert, K. Bethge, and K.-O. Pfeiffer, Nucl. Phys. **A110**, 142 (1968).
[11] M. Makowska-Rzeszutko, P. Egelhof, D. Kassen, E. Steffens, W. Weiss, and D. Fick, Phys. Lett. **74B**, 187 (1978).
[12] J. Meyer, R.S. Nahabetian, and E. Elbaz, J. Phys. (Paris) Lett. **39**, L158 (1978).
[13] N.F. Mangelson, B.G. Harvey, and N.K. Glendenning, Nucl. Phys. **A117**, 161 (1968).
[14] F.D. Santos, B.C. Karp, J.E. Bowsher, E.J. Ludwig, and A.M. Eiró, Phys. Rev. C **32**, 338 (1985).
[15] C.M. Bhat, Y. Tagishi, E.J. Ludwig, and B.A. Brown, Phys. Rev. C **34**, 736 (1986).
[16] A.J. Mendez, E.G. Myers, K.W. Kemper, P.L. Kerr, E.L. Reber, and B.G. Schmidt, Nucl. Instrum. Methods A **329**, 37 (1993).
[17] E.G. Myers, A.J. Mendez, K.W. Kemper, and B.G. Schmidt, Nucl. Instrum. Methods B **56/57**, 1156 (1991).
[18] A.J. Mendez, P.V. Green, K.W. Kemper, P.L. Kerr, E.G. Myers, E.L. Reber, and B.G. Schmidt, Nucl. Phys. **A567**, 655 (1994).
[19] M.F. Vineyard, J. Cook, K.W. Kemper, and M.N.

Stephens, Phys. Rev. C **30**, 916 (1984).
[20] *Polarization Phenomena in Nuclear Reactions*, edited by H.H. Barschall and W. Haeberli (University of Wisconsin Press, Madison, 1971).
[21] F.D. Santos and A.M. Eiró, Port. Phys. **15**, 65 (1984).
[22] K. Amos, D. Koetsier, and D. Kurath, Phys. Rev. C **40**, 374 (1989).
[23] S. Cohen and D. Kurath, Nucl. Phys. **73**, 1 (1965).
[24] R.L. Huffman, J. Dubach, R.S. Hicks, and M.A. Plum, Phys. Rev. C **35**, 1 (1987).
[25] I. Talmi, Phys. Rev. C **39**, 284 (1989).
[26] B. Jancovici and I. Talmi, Phys. Rev. **95**, 289 (1954).
[27] D.R. Inglis, Rev. Mod. Phys. **25**, 390 (1953).
[28] C. Bennhold and L. Tiator, Phys. Rev. C **42**, 464 (1990).
[29] E. Fabrici, S. Micheletti, M. Pignanelli, and F.G. Resmini, Phys. Rev. C **21**, 844 (1980).
[30] M.F. Werby, M.B. Greenfield, K.W. Kemper, D.L. McShan, and S. Edwards, Phys. Rev. C **8**, 106 (1973).
[31] P.D. Kunz, computer code DWUCK5, unpublished.
[32] E.L. Reber, K.W. Kemper, P.V. Green, P.L. Kerr, A.J. Mendez, E.G. Myers, and B.G. Schmidt, Phys. Rev. C **49**, R1 (1994).
[33] J. Lowe and A.R. Barnett, Nucl. Phys. **A187**, 323 (1972).
[34] W.W. True, Phys. Rev. **130**, 1530 (1963).
[35] Y. Hirabayashi and Y. Sakuragi, Nucl. Phys. **A536**, 375 (1992), and references contained therein.
[36] J.E. Bowsher, T.B. Clegg, H.J. Karwowski, E.J. Ludwig, W.J. Thompson, and J.A. Tostevin, Phys. Rev. C **45**, 2824 (1992).
[37] E.L. Reber, K.W. Kemper, P.V. Green, P.L. Kerr, A.J. Mendez, E.G. Myers, B.G. Schmidt, and V. Hnizdo, Phys. Rev. C **50**, 2917 (1994).